UvA-DARE (Digital Academic Repository)

An Anion-Exchange Membrane Fuel Cell Containing Only Abundant and Affordable Materials

Biemolt, J.; Douglin, J.C.; Singh, R.K.; Davydova, E.S.; Yan, N.; Rothenberg, G.; Dekel, D.R.

Citation for published version (APA):

An Anion-Exchange Membrane Fuel Cell Containing Only Abundant and Affordable Materials

Jasper Biemolt, John C. Douglin, Ramesh K. Singh, Elena S. Davydova, Ning Yan,* Gadi Rothenberg,* and Dario R. Dekel*

Herein, a unique anion-exchange membrane fuel cell (AEMFC) containing only affordable and abundant materials is presented: NiFe hydrogen oxidation reaction (HOR) and nitrogen-doped carbon oxygen reduction reaction (ORR) electrocatalysts. AEMFCs are an attractive alternative to proton-exchange membrane fuel cells. They can run under alkaline conditions, allowing the use of platinum group metal (PGM)-free electrocatalysts. Yet, the same alkaline conditions incur an overpotential loss in ORR and also slow the HOR. This can be solved by using PGM electrodes, but then the original advantage disappears. In contrast, the fuel cell is free of both PGMs and critical raw materials (CRMs). Electrochemical studies confirmed that the catalysts are highly active in both HOR and ORR in an alkaline electrolyte. The morphology, composition, and chemical states of the electrocatalysts are characterized by different techniques, including scanning electron microscopy (SEM), transmission electron microscopy (TEM), X-ray photoelectron spectroscopy (XPS), X-ray diffraction (XRD), and electron energy loss spectroscopy (EELS). Then, the electrocatalysts' performance is tested in a fuel cell device. The cell gives a maximum power density of 56 mW cm^{-2} and a limiting current density of 220 mA cm^{-2}. These results are among the best CRM-free anion-exchange membrane fuel cells reported to date.

Sustainable chemistry and sustainable energy are popular buzzwords, yet they require viable technological concepts to become reality. As such, anion-exchange membrane fuel cells (AEMFCs) have attracted much attention lately due to their potential for avoiding platinum group metal electrocatalysts.[1–4] Achieving this platinum group metal (PGM)-free goal, however, is extremely challenging. From all studies showing AEMFC performance data, only 6% are based on platinum-free electrocatalysts and very few of those are completely PGM-free.[5,6] The first to report such cell performance were Lu et al.,[7] who showed in 2008 a Ni–Cr anode

and Ag cathode AEMFC with a promising peak power density of 50 mW cm^{-2}. Five years later, two more studies achieved peak power densities of 76 and 40 mW cm^{-2}, using AEMFCs based on Ni/Ag and NiW/CoPPY-based (anode/cathode) electrocatalysts, respectively.[8,9] Since then, the only report of an AEMFC based on PGM-free electrocatalysts used NiCo/C and Co$_3$O$_4$/C, with a peak power density of 22 mW cm^{-2}.[10] While these pioneering studies showed the feasibility of PGM-free electrocatalysts, most still use critical raw materials (CRMs) such as cobalt, chromium, and tungsten.[11,12]

Any large-scale and sustainable deployment of AEMFCs should minimize the use of both PGMs and CRMs.[13] With this in mind, we focused our research on CRM-free electrocatalysts, aiming at demonstrating their feasibility in AEMFC performance tests. The Technion group showed previously that Ni$_3$Fe-based electrocatalysts are highly active for the hydrogen oxidation reaction (HOR) in alkaline conditions,[14] and that Ni$_3$Fe/C HOR electrocatalysts are stable in alkaline media.[15] Elsewhere, the UvA group demonstrated the utility of metal-free nitrogen-doped carbon catalysts for the oxygen reduction reaction (ORR) electrodes. In this communication, we combine a similar Ni$_x$Fe HOR catalyst and the ORR catalyst in a complete fuel cell, presenting an affordable and abundant electrocatalyst system for AEMFCs.

For the HOR catalyst, we built on our studies of Ni$_3$Fe/C, which showed a negligible dissolution up to 0.7 V$_{RHE}$.[15] This catalyst maintained its HOR activity after 1000 cycles to 0.3

J. Biemolt, Dr. N. Yan, Prof. G. Rothenberg
Van 't Hoff Institute for Molecular Sciences
University of Amsterdam
Science Park 904, XH Amsterdam 1098, The Netherlands
E-mail: n.yan@uva.nl; g.rothenberg@uva.nl

The ORCID identification number(s) for the author(s) of this article can be found under https://doi.org/10.1002/ente.202000909.

J. C. Douglin, Dr. R. K. Singh, Dr. E. S. Davydova, Prof. D. R. Dekel
The Wolfson Department of Chemical Engineering
Technion – Israel Institute of Technology
Technion City, Haifa 3200003, Israel
E-mail: dario@technion.ac.il

Dr. R. K. Singh, Prof. D. R. Dekel
The Nancy & Stephen Grand Technion Energy Program (GTEP)
Technion – Israel Institute of Technology
Technion City, Haifa 3200003, Israel

V_{RHE}, comparing favorably with Ni$_3$Mo/C and Ni$_3$Cu/C.[16,17] We therefore opted for developing nickel-rich NiFe bimetallic HOR electrocatalysts. A nominal Ni$_7$Fe stoichiometry was chosen to increase the nickel content in the bimetallic nanoparticle, aiming for high HOR activity while still keeping some iron in the particles for chemical and electrochemical stability. The Ni$_7$Fe/C anodes were prepared by first mixing the salts of Ni and Fe in a nominal 7:1 molar ratio, followed by wet chemical reduction with sodium borohydride.[14,15] This yields a uniform dispersion of Ni$_7$Fe/C of size ≈10–15 nm.

As the ORR catalyst, we used nitrogen-doped carbon,[18] a family of materials known for their excellent ORR activity in alkaline conditions.[19–22] This material is easily made on a multigram scale and can be tailored to specific operating conditions.[23,24] Briefly, the material was prepared by first forming a magnesium–nitrilotriacetic acid metal–organic framework. This was then carbonized, acid washed to remove any MgO and form hierarchical pores, and recarbonized (see Supporting Information for detailed experimental procedures).

The Ni/Fe atomic ratio, measured by inductively coupled plasma atomic emission spectroscopy (ICP-AES), was ≈8.5, confirming the nickel-rich content. **Figure 1** shows the physical and chemical characterizations of the Ni$_7$Fe/C and N-doped carbon electrocatalysts. The scanning transmission electron microscope high-angle annular dark-field imaging (STEM-HAADF) image and the corresponding energy-dispersive X-ray spectroscopy (EDS) elemental maps of Ni$_7$Fe/C for Ni, Fe, O, and C are shown in Figure 1a–e. The particle size of the N$_7$iFe alloy is ≈10–15 nm, with a fine mixing of the metals. From the single nanoparticle HAADF images, we estimate a uniform oxide layer coating of ≈3.6 nm. The oxide content is slightly higher than that reported for Ni$_3$Fe nanoparticles.[14,15] Several studies state that the presence of metal–metal oxide phase is important for alkaline HOR catalysis.[25–27] The core/shell structure shown in the HAADF images also reflects the surface segregation, suggesting that detailed surface analysis (e.g., by X-ray photoelectron spectroscopy [XPS]; see later) is useful. Additional morphological data are shown in Figure S1 and S2, Supporting Information. These observations are supported by cross-analysis using electron energy loss spectroscopy (EELS; see maps and spectra in Figure S3, Supporting Information). The peak at high energy loss regions at 531 eV, doublet at 708/721 eV, and the doublet at 853/872 eV correspond to O, Fe L$_{2,3}$, and Ni L$_{2,3}$, respectively, due to inner electron transition and suggests that Fe and Ni nanoparticles are at least partially oxidized.[28]

Figure 1f shows the SEM image of the N-doped carbon. The flakes are a few microns in diameter, with a macroporous network that enables a fast mass transfer. TEM reveals mesopores within the structure, further expanding the network. The material has a high specific surface area of 1320 m^2 g^{-1} and ample pore volume (3.10 cm^3 g^{-1} in total, of which 80% comes from mesopores). Its nitrogen content is 4.6 wt%, of which 36% pyridinic, 51% graphitic, and 14% oxidized. A detailed study of the morphology and surface composition of this material is published elsewhere.[18,24]

The X-ray diffraction (XRD) pattern of Ni$_7$Fe/C, shown in Figure S4a, Supporting Information, suggests an amorphous phase (similar patterns were reported for Ni$_3$Fe/C prepared by the same synthesis protocol).[15] We see a dominant peak at $2\theta = 45.34°$, which is higher than the counterpart of the pure Ni (JCPDS #00-004-0850), Fe (JCPDS #00-006-0696), and Ni-Fe (JCPDS #00-037-0474) phases. This also suggests lattice contraction, in contrast to Ni$_3$Fe/C, where lattice expansion was observed.[14,15]

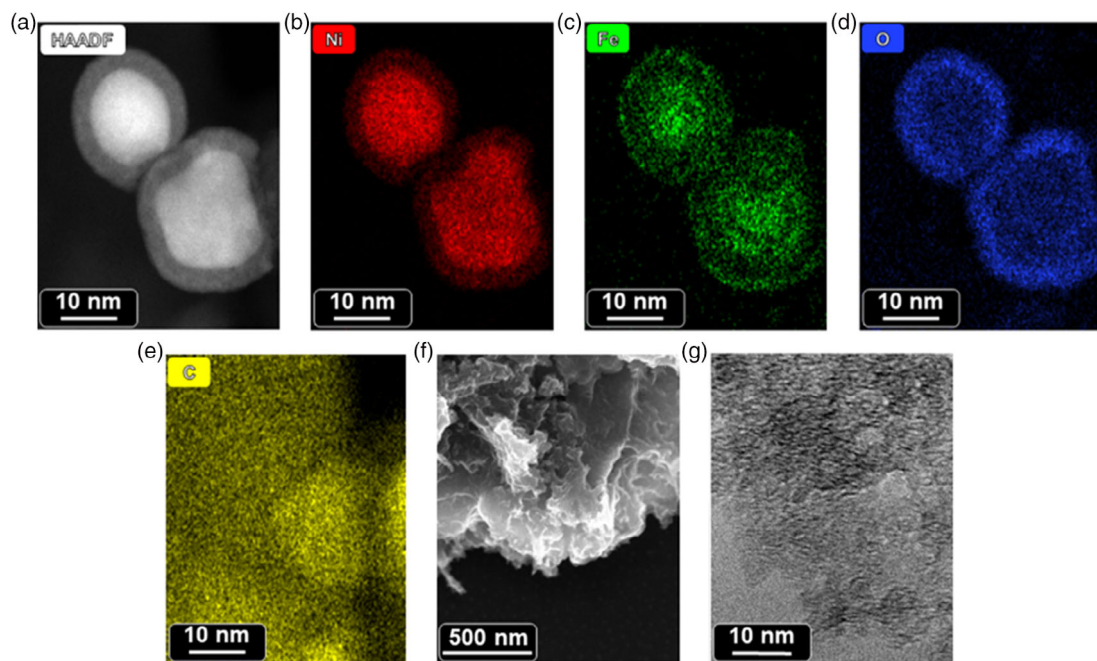**Figure 1.** Catalyst characterization: a) HAADF image of Ni$_7$Fe/C; b–e) STEM-EDS maps of Ni$_7$Fe/C; f) scanning electron microscopy (SEM) of the N-doped carbon; and g) transmission electron microscopy (TEM) of the N-doped carbon.

ADVANCED
SCIENCE NEWS
www.advancedsciencenews.com

Energy Technology
Generation, Conversion, Storage, Distribution

www.entechnol.de

The Ni2p XPS spectrum of Ni_7Fe/C is shown in Figure S4b, Supporting Information (the full survey spectrum is shown Figure S5 and Tables S1 and S2, Supporting Information). We see that the Ni:Fe surface atom ratio equals 15.3. The peak at 853.72 eV is at a binding energy close to Ni^0. As the Ni $2p_{3/2}$ peak position in Ni–Fe alloy is nearly identical to that of Ni^0, this peak relates to a Ni–Fe alloying component.[29] NiO is usually reported at about 854.5 eV, although some references relate this peak to 856.0 eV binding energy.[15] Therefore, the peak at 853.72 eV can be attributed to a NiO_x phase, with "x" slightly lower than unity (e.g., NiO with some defects: O-deficiency/vacancies). The peak at 856.2 eV is rather broad as it includes several components. We assign it to $Ni_2O_3 + Ni(OH)_2$. Similarly, the peak at 858.1 eV is assigned to Ni–O–Fe. Elsewhere, the same component was found at a slightly higher binding energy of 858.8 eV.[15] Conversely, $NiFe_2O_4$ gives this peak at about 855.0 eV.[30] Therefore, the exact energy position of Ni–O–Fe depends on the composition, $Ni_xFe_yO_z$. Note that the Fe 2p (707, 720 eV doublet) interacts with the Ni LMM structure (706, 712 eV). The Fe concentration is 15× lower than Ni, perhaps not even as high as C and O. Therefore, measuring Fe 2p may be challenging. We also see a NiB phase from the XPS spectra of B1s (Figure S5, Supporting Information), which is mainly due to the reduction process using $NaBH_4$.[31,32]

We then characterized both the Ni_7Fe/C and N-doped carbon electrocatalysts using rotating disk electrode (RDE) tests (**Figure 2**; see experimental section for details). The HOR polarization curve of Ni_7Fe/C is shown in Figure 2a. The corresponding cyclic voltammetry (CV) in Ar-saturated electrolyte is shown in the inset of Figure 2a, to estimate the electrochemical active surface area (ECSA; see Supporting Information). Figure S6, Supporting Information, shows the HOR CV of Ni_7Fe/C, suggesting a significant increase in current in H_2-saturated solution as compared with CV in an Ar-saturated solution. The specific exchange current ($i_{o,m}$) is calculated to be 3.90 mA mg^{-1}_{cat}, which is further increased by normalizing with the Ni loading estimated from ICP-AES as 7.9 mA mg^{-1}_{Ni}. The exchange current density ($j_{o,s}$) is estimated to be 0.032 mA cm^{-2}_{Ni}, which is comparable with the Ni-based catalysts reported by Yang et al.[25] and higher than the previous reports.[16,17,33–35] Elsewhere, studying analogous Ni-based electrocatalysts, we suggested that the HOR is influenced by both the hydrogen and hydroxide binding energies, and that the HOR activity of Ni_3Fe/C is due to higher OH^- coverage at lower overpotentials.[14] We believe that a similar case applies to this Ni_7Fe/C catalyst.

Figure 2b shows the LSV curve of the N-doped carbon ORR electrocatalyst measured at different angular velocities in a 0.1 M KOH electrolyte. The ORR onset potential is 0.91 V_{RHE} and the halfwave potential is 0.81 V_{RHE}. Previously, we established that the current in this potential range comes from the oxygen reduction reaction, by performing a similar measurement in N_2-saturated electrolyte.[24] The combination of the aforementioned nitrogen active sites and pore structure also yields a high electron transfer number of 3.64, indicating an almost full reduction of O_2 to H_2O. The corresponding Koutecký–Levich calculations and a table comparing this N-doped carbon to other metal-free ORR catalysts are available elsewhere.[18,24]
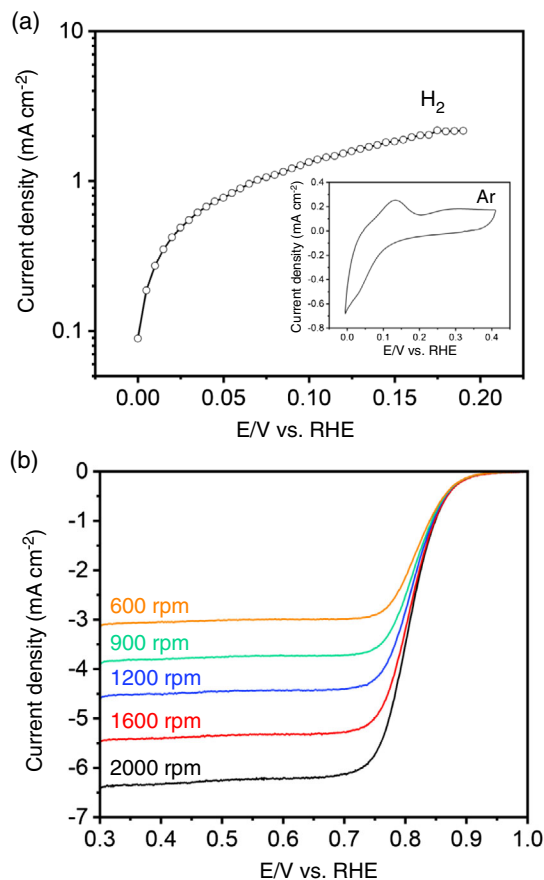

Figure 2. HOR polarization curve of Ni_7Fe/C electrocatalyst. a) Inset shows the corresponding CV in Ar-saturated 0.1 M KOH and b) ORR linear sweep voltammograms (LSV) of the N-doped carbon electrocatalyst. HOR: 1.0 M KOH with 1 mV s^{-1} and 1600 rpm, and ORR: 0.1 M KOH with 10 mV s^{-1}.

Finally, we tested the two electrocatalysts in an AEMFC setup. A 5 cm^2 electrochemical cell was assembled by pressing a Ni_7Fe/C electrocatalyst-coated membrane anode onto an N-doped carbon electrocatalyst gas diffusion electrode cathode (see photo and schematic in **Figure 3**, as well as electrode preparation photos in Figure S7, Supporting Information). Figure 3c shows the resulting polarization curve of the cell. This cell shows promising performance with a maximum power density of 56 mW cm^{-2} at a current density of 138 mA cm^{-2}. In particular, the cell achieved a limiting current density higher than 200 mA cm^{-2}. This remarkable current density value is the highest reported to date (in fact, it is double the limiting current densities reported for AEMFCs using CRM-containing electrocatalysts in both the anode and the cathode; see Table S3, Supporting Information).

We have built a completely PGM-free and CRM-free anion-exchange membrane fuel cell using Ni_7Fe/C and N-doped carbon electrocatalysts. The cell achieved a maximum power density of 56 mW cm^{-2} at a current density of 138 mA cm^{-2}, which are among the highest values reported to date for CRM-free electrocatalyst systems. We believe that CRM-free fuel cells are the only viable option for a large-scale, long-term, and sustainable energy transition. However, such a transition also requires solutions
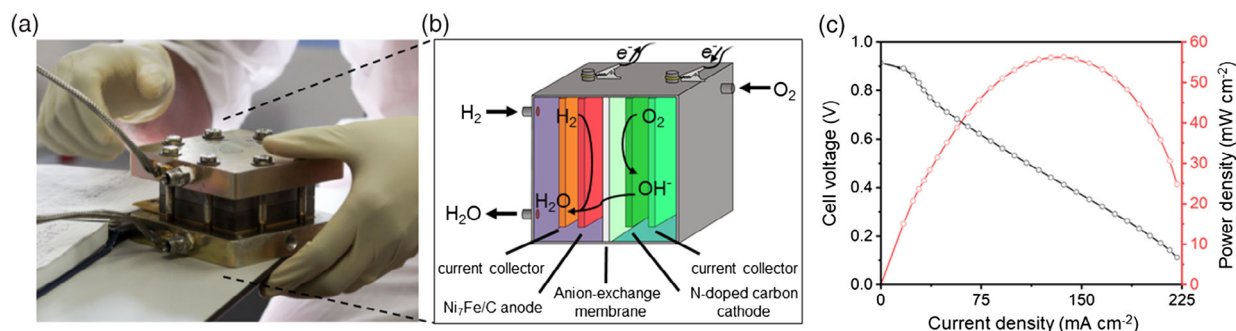
Figure 3. a) Photo and b) schematic of the AEMFC setup. c) Polarization curve of the AEMFC with Ni$_7$Fe/C anode and N-doped carbon cathode catalysts. $T_{cell} = 95\,°C$, RH of 100%, flow rates of 0.01 L min^{-1} of H$_2$ (2 barg) and 0.2 L min^{-1} of O$_2$ (no back pressure) for anode and cathode, respectively.

using known concepts and techniques, limiting the need for new production lines and methods. Our electrocatalysts fit these criteria, with straightforward and scalable preparation protocols (all detailed experimental procedures are included in the Supporting Information). As such, we hope that the publication of these results will inspire others in developing sustainable and long-term solutions for the energy transition challenge problems facing our future.

Supporting Information

Supporting Information is available from the Wiley Online Library or from the author.

Conflict of Interest

The authors declare no conflict of interest.

Data Availability Statement

Research data are not shared.

[1] B. P. Setzler, Z. Zhuang, J. A. Wittkopf, Y. Yan, *Nat. Nanotechnol.* **2016**, *11*, 1020.

[2] E. Agel, J. Bouet, J. F. Fauvarque, *J. Power Sources* **2001**, *101*, 267–274.

[3] J. R. Varcoe, P. Atanassov, D. R. Dekel, A. M. Herring, M. A. Hickner, P. A. Kohl, A. R. Kucernak, W. E. Mustain, K. Nijmeijer, K. Scott, T. Xu, L. Zhuang, *Energy Environ. Sci.* **2014**, *7*, 3135.

[4] S. Gottesfeld, D. R. Dekel, M. Page, C. Bae, Y. Yan, P. Zelenay, Y. S. Kim, *J. Power Sources* **2018**, *375*, 170–184.

[5] D. R. Dekel, *J. Power Sources* **2018**, *375*, 158.

[6] X. Peng, V. Kashyap, B. Ng, S. Kurungot, L. Wang, J. Varcoe, W. Mustain, *Catalysts* **2019**, *9*, 264.

[7] S. Lu, J. Pan, A. Huang, L. Zhuang, J. Lu, *Proc. Natl. Acad. Sci. U. S. A.* **2008**, *105*, 20611.

[8] Q. Hu, G. Li, J. Pan, L. Tan, J. Lu, L. Zhuang, *Int. J. Hydrog. Energy* **2013**, *38*, 16264.

[9] S. Gu, W. Sheng, R. Cai, S. M. Alia, S. Song, K. O. Jensen, Y. Yan, *Chem. Commun.* **2013**, *49*, 131.

[10] V. Men Truong, J. Richard Tolchard, J. Svendby, M. Manikandan, H. A. Miller, S. Sunde, H. Yang, D. R. Dekel, A. Oyarce Barnett, *Energies* **2020**, *13*, 582.

[11] A. Chapman, J. Arendorf, T. Castella, P. Thompson, P. Willis, L. T. Espinoza, S. Klug, E. Wichman, *Study on Critical Raw Materials at EU Level – Final Report*, European Commission, **2013**.

[12] S. M. Fortier, N. T. Nassar, G. W. Lederer, J. Brainard, J. Gambogi, E. A. McCullough, *Draft Critical Mineral List—Summary of Methodology and Background Information—U.S. Geological Survey Technical Input Document in Response to Secretarial Order No. 3359*, U.S. Geological Survey, Reston, VA **2018**.

[13] T. Asefa, X. Huang, *Chem. – Eur. J.* **2017**, *23*, 10703.

[14] E. Davydova, J. Zaffran, K. Dhaka, M. Toroker, D. Dekel, *Catalysts* **2018**, *8*, 454.

[15] E. S. Davydova, F. D. Speck, M. T. Y. Paul, D. R. Dekel, S. Cherevko, *ACS Catal.* **2019**, *9*, 6837.

[16] S. Kabir, K. Lemire, K. Artyushkova, A. Roy, M. Odgaard, D. Schlueter, A. Oshchepkov, A. Bonnefont, E. Savinova, D. C. Sabarirajan, P. Mandal, E. J. Crumlin, I. V. Zenyuk, P. Atanassov, A. Serov, *J. Mater. Chem. A* **2017**, *5*, 24433.

[17] A. G. Oshchepkov, P. A. Simonov, O. V. Cherstiouk, R. R. Nazmutdinov, D. V. Glukhov, V. I. Zaikovskii, T. Yu. Kardash, R. I. Kvon, A. Bonnefont, A. N. Simonov, V. N. Parmon, E. R. Savinova, *Top. Catal.* **2015**, *58*, 1181.

[18] D. Eisenberg, W. Stroek, N. J. Geels, C. S. Sandu, A. Heller, N. Yan, G. Rothenberg, *Chem. – Eur. J.* **2016**, *22*, 501.

[19] J. Zhang, Z. Zhao, Z. Xia, L. Dai, *Nat. Nanotechnol.* **2015**, *10*, 444.

[20] H. Jiang, J. Gu, X. Zheng, M. Liu, X. Qiu, L. Wang, W. Li, Z. Chen, X. Ji, J. Li, *Energy Environ. Sci.* **2019**, *12*, 322.

[21] J. Tang, J. Liu, C. Li, Y. Li, M. O. Tade, S. Dai, Y. Yamauchi, *Angew. Chem., Int. Ed.* **2015**, *54*, 588.

[22] D. Guo, R. Shibuya, C. Akiba, S. Saji, T. Kondo, J. Nakamura, *Science* **2016**, *351*, 361.

[23] J. Biemolt, G. Rothenberg, N. Yan, *Inorg. Chem. Front.* **2020**, *7*, 177.

[24] D. Eisenberg, P. Prinsen, N. J. Geels, W. Stroek, N. Yan, B. Hua, J.-L. Luo, G. Rothenberg, *RSC Adv* **2016**, *6*, 80398.

[25] F. Yang, X. Bao, P. Li, X. Wang, G. Cheng, S. Chen, W. Luo, *Angew. Chem., Int. Ed.* **2019**, *58*, 14179.

[26] Y. Yang, X. Sun, G. Han, X. Liu, X. Zhang, Y. Sun, M. Zhang, Z. Cao, Y. Sun, *Angew. Chem., Int. Ed.* **2019**, *58*, 10644.

[27] A. G. Oshchepkov, A. Bonnefont, V. A. Saveleva, V. Papaefthimiou, S. Zafeiratos, S. N. Pronkin, V. N. Parmon, E. R. Savinova, *Top. Catal.* **2016**, *59*, 1319.

[28] R. H. Manso, P. Acharya, S. Deng, C. C. Crane, B. Reinhart, S. Lee, X. Tong, D. Nykypanchuk, J. Zhu, Y. Zhu, L. F. Greenlee, J. Chen, *Nanoscale* **2019**, *11*, 8170.

[29] Y. Nagai, M. Senda, T. Toshima, *Jpn. J. Appl. Phys.* **1987**, *26*, L1131.

[30] L. Marchetti, F. Miserque, S. Perrin, M. Pijolat, *Surf. Interface Anal.* **2015**, *47*, 632.

[31] J. Legrand, S. Gota, M.-J. Guittet, C. Petit, *Langmuir* **2002**, *18*, 4131.

[32] Y. Chen, L. Liu, Y. Wang, H. Kim, *Fuel Process. Technol.* **2011**, *92*, 1368.

[33] Z. Zhuang, S. A. Giles, J. Zheng, G. R. Jenness, S. Caratzoulas, D. G. Vlachos, Y. Yan, *Nat. Commun.* **2016**, *7*, 10141.

[34] A. Roy, M. R. Talarposhti, S. J. Normile, I. V. Zenyuk, V. De Andrade, K. Artyushkova, A. Serov, P. Atanassov, *Sustain. Energy Fuels* **2018**, *2*, 2268.

[35] W. Sheng, A. P. Bivens, M. Myint, Z. Zhuang, R. V. Forest, Q. Fang, J. G. Chen, Y. Yan, *Energy Environ. Sci.* **2014**, *7*, 1719.